Computer Simulation of Polydisperse Liquids with Density- and Temperature-Dependent Distributions†

Michael R. Stapleton, Dominic J. Tildesley,*

Department of Chemistry, The University, Southampton, S09 5NH, UK

Timothy J. Sluckin,‡

Faculty of Mathematics The University, Southampton, S09 5NH, UK

and Nicholas Quirke

BP Research Centre, Chertsey Road, Sunbury on Thames, London, UK *(Received: November 2, 1987)*

This paper presents a Monte Carlo simulation method for studying liquid mixtures which are polydisperse. If we consider the case of polydispersity in the particle size σ, the method requires the low-density distribution of sizes $F_u(\sigma)$ corresponding to the polydispersity of isolated particles. It predicts how the size distribution changes with density and temperature. This phenomenon of variable polydispersity is applicable to micellar systems, microemulsions, hydrocarbon fluids and solutions. In this paper we study a number of model forms for $F_u(X)$ which are Schultz distributions. Intermolecular interactions are described by using a hard-sphere or Lennard-Jones potential, and the polydisperse variable X is the particle diameter, σ, or well-depth, ϵ. In the case of the hard-sphere potential, the average particle size decreases as the density is increased. When there are attractive interactions between particles, the average size increases as density is increased and then decreases. In systems involving a small to moderate degree of polydispersity, the structure and thermodynamic properties of the fluid can be represented by those of a monodisperse fluid at the same packing fraction, which can be calculated from the third moment of the final distribution $F(\sigma)$. A theoretical approach to the prediction of the moments of $F(\sigma)$ in the case of variable polydispersity is developed.

1. Introduction

In recent years the theoretical techniques which have successfully described simple atomic fluids have been extended to model the behavior of polydisperse fluids. The solution of the Percus Yevick approximation for a multicomponent mixture of hard spheres[1] has been generalized to a hard-sphere fluid where the atomic diameters, σ, are polydisperse.[2,3] The scattering functions of the polydisperse hard-sphere and permeable sphere fluids have been calculated,[4,5] and a formal diagramatic expansion of the properties of polydisperse fluids has been developed.[6,7] Attractive interactions can be added to these models by using thermodynamic perturbation theory, and liquid–vapor coexistence curves have been calculated.[2,8,9]

To complement these theoretical developments, there have been a number of simulation studies of polydispersity. In these simulations some characteristic parameter, X, of the atoms is chosen from a particular distribution function $F(X)$. X might be the atom diameter and $F(X_0)\ dX_0$ represents the fraction of atoms with diameters in the range X_0 to $X_0 + dX_0$. This initial distribution is fixed for the simulation, and constant-NVT Monte Carlo (MC) or constant-NVE molecular dynamics (MD) are used to calculate the properties of the fluid. The structure factor for polydisperse hard spheres has been calculated by using MC.[10] A model fluid with a double-layer repulsion and a Hamaker attraction has been studied by using MC[11] and MD,[12] and a solid–fluid phase transition induced by continuously varying the degree of polydispersity.[13] Phase separation in a polydisperse mixture of hard disks with nonadditive diameters has also been simulated.[14]

In these studies, once $F(X)$ is defined, we can use simulation or theory to calculate the properties of the fluid. We call this type of behavior "fixed" polydispersity. Certain colloidal systems, such as synthesized latex spheres, exhibit this kind of behavior. The characteristic feature of fixed polydispersity is that $F(X)$ is independent of the density and temperature.

In nature we find another important type of behavior, which we can label "variable" polydispersity. Here the distribution $F(X)$ changes with density and temperature. An example of this kind of system would be a fluid of nonionic micelles formed from an alkyl poly(oxyethylene) surfactant in water. One such surfactant, C_8E_4, is known to form spherical micelles above the critical micelle concentration.[15] Theoretical and experimental studies indicate that these micelles are likely to be polydisperse in size[16] with the degree of polydispersity determined by factors such as head-group repulsion, and the amount of bound water associated with each head group, and the isomeric states of the hydrocarbon chains. We call this "low-density distribution" of sizes the underlying distribution of the fluid. As the density of the micellar fluid increases by the removal of water, the micellar particles begin to interact more strongly and the intermicellar forces will change the distribution of micellar sizes. A simple picture of this change would be the growth or shrinkage of the micelle in the external field of its neighbors. Growth may be enhanced by the inclusion of some free amphiphile from the solution into the micelle or the addition of tightly bound water to the head groups. It is clear during this process that a change in the distribution of micellar sizes will be coupled to a change in the distribution of a well-depth parameter which governs the magnitude of the intermicellar interactions. Changes in temperature will also have a significant

† This paper is a delayed contribution to the Rahman Festschrift.

‡ Present address: Institut Laue-Langevin 156X, 38042 Grenoble Cedex, France.

(1) Baxter, R. J. *J. Chem. Phys.* **1970**, *52*, 4559.
(2) Salacuse, J. J. Ph.D. Thesis, State University of New York at Stony Brook, 1978.
(3) Salacuse, J. J.; Stell, G. *J. Chem. Phys.* **1982**, *77*, 3714.
(4) van Beurten, P.; Vrij, A. *J. Chem. Phys.* **1981**, *74*, 2744.
(5) Blum, L.; Stell, G. *J. Chem. Phys.* **1979**, *71*, 42.
(6) Briano, J. G.; Glandt, E. D. *J. Chem. Phys.* **1984**, *80*, 3336.
(7) Briano, J. G.; Glandt, E. D. *Fluid Phase Equilib.* **1983**, *14*, 9.
(8) Gaultieri, J. A.; Kincaid, J. M.; Morrison, G. *J. Chem. Phys.* **1982**, *77*, 521.
(9) Johnson, K. A.; Jonah, D. A.; Kincaid, J. M.; Morrison, G. *J. Chem. Phys.* **1985**, *82*, 5178.
(10) Frenkel, D.; Vos, R. J.; de Kruif, C. G.; Vrij, A. *J. Chem. Phys.* **1986**, *84*, 4624.
(11) Dickinson, E. *Faraday Discuss. Chem. Soc.* **1978**, *65*, 127.
(12) Dickinson, E. *Chem. Phys. Lett.* **1978**, *57*, 148.
(13) Dickinson, E.; Parker, R.; Lal, M. *Chem. Phys. Lett.* **1981**, *79*, 578.
(14) Dickinson, E. *Chem. Phys. Lett.* **1979**, *66*, 500.
(15) Hayter, J. B.; Zulaf, M. *Colloid Polym. Sci.* **1982**, *260*, 1023.
(16) Israelachvili, J. N.; Mitchell, D. J.; Ninham, B. W. *J. Chem. Soc., Faraday Trans. 2* **1976**, *72*, 1525.

0022-3654/88/2092-4788$01.50/0

effect on the underlying distribution function.

Other surfactant systems, $C_{12}E_4/H_2O$, are thought to be composed of nonspherical micelles.[17] A similar view applies to these systems but we would need to consider an additional polydispersity in the length to breadth ratio of the prolate spherocylinder which describes the micellar shape and a corresponding polydispersity in the anisotropy of the attractive interactions. In this case the intramicellar energy and the low-density distribution of sizes would be influenced by factors such as the curvature in the spherical caps, and the relief of the curvature in the cylindrical portion of the micelles. Gelbart and co-workers have developed a theoretical approach to this problem.[18]

Micelles are not the only important systems to exhibit variable polydispersity. Oil/water emulsions, liquid foams, and blood all contain flexible particles which can distort under the influence of their neighbors because of the low interfacial tension at the boundary of the particle and the solvent.[19-21] Another interesting example is a fluid of colloidal particles, where each particle is surrounded by a sheath of soft polymer and solvent. Such a system is a dispersion in an *n*-alkane of silica particles coated with C_{18} chains (silica-*g*-stearyl).[22] Solutions containing long-chain hydrocarbons at densities below entanglement can also be thought of as exhibiting variable polydispersity. The underlying distribution corresponds to an isolated hydrocarbon chain in a solvent which is perturbed as the density increases. The difficulty in this case is finding one or two simple geometrical measures which can be used to describe the complicated variety of shapes exhibited by these chain molecules, and which can be used as independent variables in the underlying distribution.

The aim of this paper is to construct some simple models of variable polydispersity and to use a Monte Carlo simulation technique to determine the properties of these model liquids. The simulation results will be used to test a simple mean-field theory of the phenomenon and the calculation of the properties of these systems from scaled particle theory. The Monte Carlo technique described is quite general and takes as its input the temperature, the number density, and the underlying or isolated particle distribution. The output from the simulation will be the structural and thermodynamic properties of the liquid, and the particle distribution at that density and temperature. For example, if the underlying distribution described particle diameters, then the third moment of the final distribution would be directly proportional to the packing fraction of the fluid at that state point. The simulation involves atoms moving and changing their size. At any one point in the simulation all the atoms have different sizes sampled from the underlying distribution function. In this sense the simulations are of truly polydisperse fluids, rather than of mixtures with a large number of components (paucidispersed or oligodispersed fluids). An approach of this type has also been adopted in a recent simulation in the semi-grand-canonical ensemble,[23] which is equivalent to variable polydispersity in the canonical ensemble. The state-dependent distribution function distinguishes the Monte Carlo calculations described in this paper from previous simulation work.[10-14]

In section 2 of this paper we outline the models for the underlying distribution functions and the intermolecular potential interactions that we use in the paper. We describe the Monte Carlo method used to study variable polydispersity. In section 3 we present the results for fluids with purely repulsive intermolecular interactions and show the effect of including attractions. We consider a number of different forms of the underlying distribution function. In section 4 we present a mean-field theory of variable polydispersity and compare the results with the MC simulations. Section 5 contains our conclusions.

2. Simulation Method

In this description of the simulation method we illustrate the principle using size polydispersity in a fluid of spherical particles whose diameters, σ, take a range of values between two limits a and b. The function $F(\sigma)$ describes the normalized probability of finding a particular particle diameter in the polydisperse liquid. At low density, where interactions between particles are negligible, the underlying distribution, $F_u(\sigma)$ is determined solely by intraparticle energy considerations and

$$F_u(\sigma) = C \exp[-\beta V_{intra}(\sigma)] \tag{2.1}$$

where C is a constant, $\beta = (kT)^{-1}$, k is Boltzmann's constant, T is the temperature, and V_{intra} is the intraparticle energy. At a particular density and temperature, where particle interactions are not negligible, the form of $F(\sigma)$ will be different from the underlying distribution $F_u(\sigma)$ because of the balance between intraparticle and interparticle free energies. The properties of this fluid can be calculated by using a Monte Carlo simulation technique.[24]

Most of the simulations reported in this paper were performed in the canonical ensemble. A single trial move involves attempting to change a particle's position and size. It is simpler to think about these steps separately, although they are combined in the program. Changes in particle positions are accomplished by using the standard Metropolis algorithm. To change the particle size we make the following choice for the underlying stochastic matrix of the Markov chain

$$\alpha_{mn} = F_u(\sigma_n)$$
$$\alpha_{nm} = F_u(\sigma_m) \tag{2.2}$$

where m and n are two consecutive states of the fluid. Since α is not symmetric the appropriate transition matrix, π_{mn}, for a change in the particle size is

$$\pi_{mn} = \alpha_{mn}, \quad \alpha_{nm}p_n \geq \alpha_{mn}p_m$$
$$\pi_{mn} = \alpha_{mn}(\alpha_{nm}p_n/\alpha_{mn}p_m), \quad \alpha_{nm}p_n < \alpha_{mn}p_m \tag{2.3}$$

where p_m and p_n are the probabilities that the fluid is in states m and n respectively.

$$p_n/p_m = \exp(-\beta\delta V^{nm}_{inter}) \exp(-\beta\delta V^{nm}_{intra})$$
$$= \exp(-\beta\delta V^{nm}_{inter})[F_u(\sigma_n)/F_u(\sigma_m)] \tag{2.4}$$

where δV^{nm} represents an energy difference between the states.

The condition of microscopic reversibility is satisfied if moves are chosen with a probability given by

$$\min[1, \alpha_{nm}p_n/\alpha_{mn}p_m]$$

or substituting eq 2.4 into eq 2.3

$$\min[1, \exp(-\beta\delta^{nm}_{inter})] \tag{2.5}$$

To apply this solution we choose a particle at random, which has a diameter σ. The intermolecular energy of the particle in its current position is determined and the particle is given a uniform random displacement to a new trial position. A trial diameter is sampled from the underlying distribution $F_u(\sigma)$ in the range $a \leq \sigma \leq b$, and the interparticle energy recalculated. A value of σ is sampled from the appropriate underlying distribution by using the von Neumann acceptance–rejection method.[25] This method is general enough to allow for a tabulated $F_u(\sigma)$.

The change in the *interparticle* energy is used in the condition (2.5) to determine whether the trial move is accepted. If the trial move is rejected, the old position and diameter are retained.

If trial diameters are sampled randomly and uniformly on the range a to b the method reduces to the conventional Metropolis

(17) Nilsson, P. G.; Lindman, B. *J. Phys. Chem.* **1984**, *88*, 4764.
(18) Ben-Shaul, A.; Gelbart, W. M. *J. Phys. Chem.* **1982**, *86*, 316.
(19) Grimson, M. J.; Honary, F. *Phys. Lett.* **1984**, *102A*, 241.
(20) Dickinson, E. *Phys. Rev. Lett.* **1984**, *53*, 728.
(21) Barker, G. C.; Grimson, M. J. *Mol. Phys.*, in press.
(22) Edwards, J.; Everett, D. H.; O'Sullivan, T.; Pangalou, I.; Vincent, B. *J. Chem. Soc., Faraday Trans. 1* **1984**, *80*, 2599.
(23) Kofke, D. A.; Glandt, E. D. *Fluid Phase Equilib.* **1986**, *29*, 327.
(24) Allen, M. P.; Tildesley, D. J. *Computer Simulation of Liquids*; Clarendon: Oxford, U.K., 1987.
(25) Rubinstein, R. Y. *Simulation and the Monte Carlo Method*; Wiley: New York, 1981.
(26) Eppenga, R.; Frenkel, D. *Mol. Phys.* **1984**, *52*, 1303.

algorithm. In some simulations we were able to use this technique, and a comparison of this conventional Metropolis and the smarter MC method (eq 2.5) shows excellent agreement. However, sampling directly from $F_u(\sigma)$ produces a markedly faster convergence. In some cases, particularly where the final distribution $F(\sigma)$ is significantly different from the underlying distribution $F_u(\sigma)$, we were unable to use the conventional method and maintain a reasonable acceptance ratio for new configurations.

In this work we have used a Schultz function as a model for the underlying distribution

$$F_u(\sigma) = (1/z!)[(z+1)/\sigma_0]^{z+1}\sigma^z \exp[-([z+1]/\sigma_0)\sigma] \qquad a \le \sigma \le b$$
$$F_u(\sigma) = 0 \qquad \text{otherwise} \tag{2.6}$$

where z is an integer which determines the width of the distribution and σ_0 is the mean value of the isolated particle diameters. This distribution has two useful features. By varying z and the range a to b in which we consider the distribution we can obtain a wide variety of shapes, from a δ function as z tends to infinity to an almost uniform distribution as z tends to zero. In addition, the moments of the Schultz function are known exactly.

$$M_j = \int_0^\infty \sigma^j F_u(\sigma)\, d\sigma = (j+z)!/[z!\{(z+1)/\sigma_0\}^j] \tag{2.7}$$

It has also been used in previous studies of polydispersity in liquids.[2,3] A disadvantage of the Schultz distribution is the complicated mathematical form which makes it difficult to use in theoretical approaches to variable polydispersity. We return to this point in section 4.

In this paper we have specifically avoided a discussion of the physics which goes into a choice of $F_u(\sigma)$ for a particular problem such as a nonionic micelle, or a microemulsion. Our aim is to develop a general technique for a range of problems. One important constraint is that the range of $F_u(\sigma)$, a to b, must be large enough to include all physically possible diameters at the temperature and density under consideration. That is, a and b must be physically reasonable bounds for $F(\sigma)$ as well as $F_u(\sigma)$. These limits are also a device to prevent the formation of unreasonably large particles in the simulation box.

We have used two common pair potentials to describe the particle interactions; the hard-sphere potential allows us to consider purely repulsive interparticle interactions

$$V(r) = \infty \qquad r < \sigma$$
$$V(r) = 0 \qquad r \ge \sigma \tag{2.8}$$

and the Lennard-Jones 12-6 potential enables us to explore the balance between attractive and repulsive forces in these polydisperse fluids

$$V(r) = 4\epsilon[(\sigma/r)^{12} - (\sigma/r)^6] \tag{2.9}$$

In both cases particle diameters are assumed to be additive

$$\sigma_{ij} = (\sigma_i + \sigma_j)/2 \tag{2.10}$$

In the simulation the normal periodic boundary conditions are applied and a spherical cutoff, Rc, of $2.5b$ (where b is the maximum particle diameter) is used in the simulation of the Lennard-Jones particles. As the size of a particle can change during a trial move, the long-range correction to the energy must be included directly in calculating δV_{nm}. The long-range correction for particle i is

$$V_{LRC} = 2\pi\rho \int_0^\infty d\sigma_j\, F(\sigma_j) \int_{R_c}^\infty dr\, v(r) r^2 \tag{2.11}$$

which can be written in terms of the moments of $F(\sigma)$

$$V_{LRC} = (\pi\rho/24R_c^3)([1/192R_c^6]\{\sigma_i^{12}M_0 + 12\sigma_i^{11}M_1 + 66\sigma_i^{10}M_2 + 220\sigma_i^9M_3 + 495\sigma_i^8M_4 + 792\sigma_i^7M_5 + 924\sigma_i^6M_6 + 792\sigma_i^5M_7 + 495\sigma_i^4M_8 + 220\sigma_i^3M_9 + 66\sigma_i^2M_{10} + 12\sigma_iM_{11} + M_{12}\} - \{\sigma_i^6M_0 + 6\sigma_i^5M_1 + 15\sigma_i^4M_2 + 20\sigma_i^3M_3 + 15\sigma_i^2M_4 + 6\sigma_iM_5 + M_6\}) \tag{2.12}$$

TABLE I: The Underlying Distribution Function F_u, i.e., the Schultz Distribution, Eq 2.6, with Lower and Upper Cutoffs at a and b[a]

function	z	a	b	M_1	M_2	M_3	τ
a	500	0.9	1.1	1.000	1.002	1.006	0.045
b	20	0.5	1.5	0.991	1.023	1.095	0.204
c	50	1.0	1.5	1.124	1.271	1.447	0.078
d	100	0.5	1.5	1.000	1.010	1.030	0.100
±				0.001	0.003	0.005	

[a] M_i is the ith moment of the underlying distribution and τ is the degree of polydispersity. The estimated errors in the determination of the first three moments in the simulations are shown in the final row.

An exact calculation of V_{LRC} requires the evaluation of the 12 moments of $F(\sigma)$ before and after each trial move. In fact, tests show that the moments of $F(\sigma)$ can be recalculated once every tenth Monte Carlo cycle, without affecting the results of the simulation. A similar equation can be obtained for the long-range correction to the pressure in terms of the moments of the final distribution.

For the Lennard-Jones model of a polydisperse liquid we also studied an energy polydispersity in which all the particles in the simulation had the same diameter σ, and the well depth ϵ is polydisperse. A Schultz function is used for the underlying distribution, $F_u(\epsilon)$. For particles with different well depths

$$\epsilon_{ij} = (\epsilon_i\epsilon_j)^{1/2} \tag{2.13}$$

The long-range correction term corresponding to eq 2.12 can be written in terms of the half-moment

$$M_{1/2} = \int_0^\infty F(\epsilon_j)\epsilon_j^{1/2}\, d\epsilon_j \tag{2.14}$$

giving

$$V_{LRC} = (8\pi\rho/9)[(1/R_c)^9 - 3(1/R_c)^3]\epsilon_i^{1/2}M_{1/2} \tag{2.15}$$

In all the simulations of size and energy polydispersity, at a particular density and temperature, $F(\sigma)$ and $F(\epsilon)$ and the first 12 moments of these distributions are calculated. An average radial distribution function, $g(r)$, is obtained. This simply represents the average number of particles at a distance r from a given particle compared with the number expected in an ideal gas at the same density and regardless of species. Energy, pressure, and chemical potential are calculated. The parameter defining the maximum displacement of the particles is continually updated so that approximately half the trial moves are accepted. A typical simulation consists of 1 million equilibration trials and 1–2 million production trials.

3. Simulation Results

In all the simulations σ_0 and ϵ_0 are set at 1.0 and we use the following reduced units $T^* = kT/\epsilon_0$, $\rho^* = \rho\sigma_0^3$, $\mu^* = \mu/\epsilon_0$, $U^* = U/\epsilon_0$, and $P^* = P\sigma_0^3/\epsilon_0$.

It is often useful to discuss the packing fraction of the fluids, which we define as $\pi\rho^*M_3/6$ for the hard-sphere and Lennard-Jones fluids.

The form of the underlying distribution is defined by the choice of the Schultz parameter z and the two limits, a and b, which determine the minimum and maximum particle size. Function a, of Table I, with $z = 500$, $a = 0.9$, and $b = 1.1$ is a narrow and almost symmetric distribution which is similar to the Gaussian distribution predicted by Israelachvili, Mitchell, and Ninham[16] for spherical micelles at the critical micelle concentration. The degree of polydispersity, τ, defined as the mean particle diameter divided by the standard deviation in the distribution of diameters, is 0.045. Function b (see Table I) with $z = 20$, $a = 0.5$, and $b = 1.5$ is a broader, less symmetric distribution with $\tau = 0.204$. Function c is essentially different from functions a and b in that the most probable diameter of an isolated particle is the minimum cutoff a. Function c is a reasonable model for the hard colloidal particle with attached chains. It is an asymmetric distribution with $z = 50$, $a = 1.0$, and $b = 1.5$ giving $\tau = 0.078$. Table I contains the first three moments of the underlying distributions.

TABLE II: Constant-NVT Simulation Results for Size Polydispersity in the Hard-Sphere Fluid[a]

ρ^*	N	M_1	M_2	M_3
		Function a		
0.0		1.000	1.002	1.006
0.005	256	1.000	1.002	1.006
0.2	256	0.998	0.997	0.998
0.4	256	0.993	0.987	0.984
0.6	256	0.985	0.972	0.961
0.85	256	0.970	0.942	0.917
		Function c		
0.0		1.124	1.271	1.447
0.005	256	1.123	1.270	1.445
0.2	256	1.107	1.231	1.377
0.2	500	1.107	1.232	1.379
0.4	256	1.085	1.181	1.291
0.6	256	1.062	1.130	1.204

[a] The moments of $F(\sigma)$ are given as a function of density for two underlying distributions.

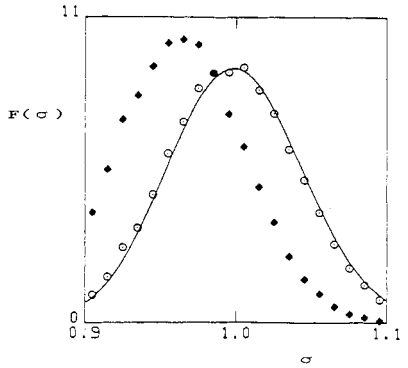

Figure 1. $F(\sigma)$ against σ for the hard-sphere fluid. The line is the underlying distribution function a, (⊙) at $\rho^* = 0.2$ and (◆) at $\rho^* = 0.85$.

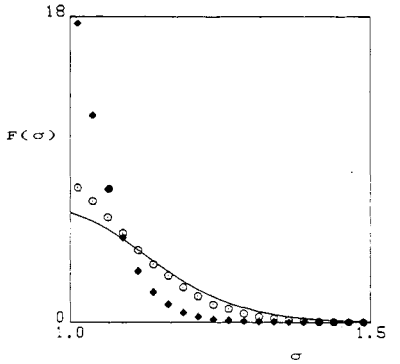

Figure 2. $F(\sigma)$ against σ for the hard-sphere fluid. The line is the underlying distribution function c, (⊙) at $\rho^* = 0.2$ and (◆) at $\rho^* = 0.6$.

We begin by considering the polydisperse hard-sphere liquid. The results for the narrow symmetric function a are given in Table II as a function of increasing density. At the low density of $\rho^* = 0.005$ we find that the distribution is unaffected by particle interactions and the moments are the same as those of $F_u(\sigma)$. As the density is increased from $\rho^* = 0.2$ to 0.85 the average particle size decreases and the form of the distribution, $F(\sigma)$, changes (see Figure 1). As the density of the fluid increases, the free energy is minimized by this reduction in the average particle diameter. The size decrease is limited by the associated increase in the intraparticle energy.

The asymmetric distribution function c shows the same trends with density as function a, see Table II. In this case the results are more pronounced because the size decrease caused by the interparticle interactions is enhanced by the form of the underlying distribution. Figure 2 shows a significant change in the form of $F(\sigma)$ at a number density of $\rho^* = 0.6$.

The chemical potential distributions, $\mu_{ex}^*(\sigma)$, can be calculated by using the Widom particle insertion method.[27] At intervals

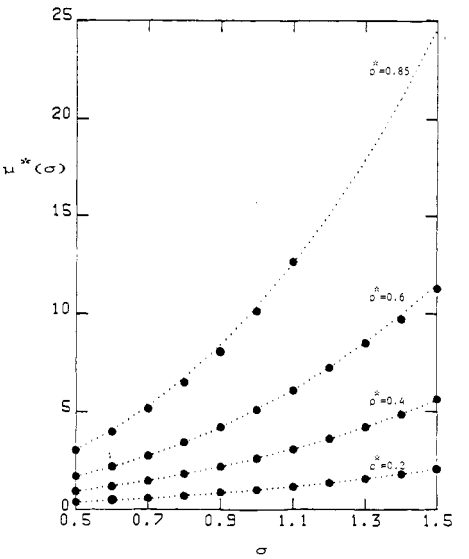

Figure 3. Chemical potential distribution for the polydisperse hard-sphere fluid (function a) as a function of density. The points are simulation results and the dotted line is the scaled particle theory of eq 3.2.

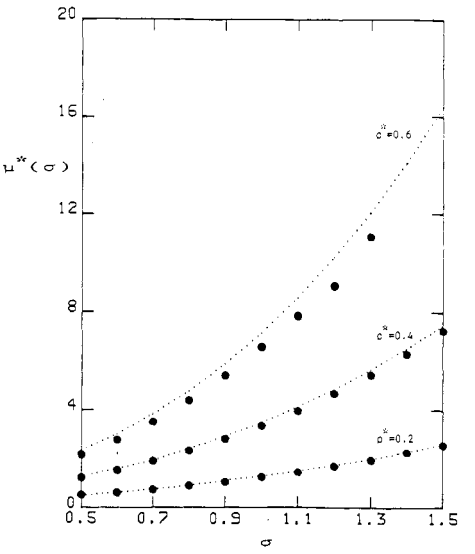

Figure 4. Chemical potential distribution for the polydisperse hard-sphere fluid (function c) as a function of density. The points are simulation results and the dotted line is the scaled particle theory of eq 3.2.

of 10 cycles an fcc lattice of 500 test particles is inserted into the fluid. The diameters of the test particles on the lattice are fixed at σ_t. The chemical potential is calculated from

$$\mu_{ex}^*(\sigma_t) = -kT \ln [\langle \exp(-V(\sigma_t)/kT) \rangle_{NVT}] \qquad (3.1)$$

where $V(\sigma_t)$ is the insertion energy for a test particle of diameter σ_t placed randomly in the liquid. For hard-core potentials the exponential in eq 3.1 is either zero or one, and the ensemble average is just the probability of a successful test particle insertion. Insertion of a range of lattices with spheres of different σ_t values produces a chemical potential distribution. The range of σ_t values is arbitrary and can include diameters which are smaller and larger than those actually found in the polydisperse hard-sphere liquid under consideration. The results are shown in Figures 3 and 4. Particle insertion fails for test lattices containing particles with large diameters since the insertion probability falls to zero. For the distribution function a we were able to calculate accurate chemical potential distribution results for diameters smaller than the maximum physical diameter b, at all densities. For distribution

(27) Widom, B. *J. Chem. Phys.* **1963**, *39*, 2808.

TABLE III: Constant-NPT Simulation Results for Size Polydispersity in the Hard-Sphere Fluid[a]

N	P/kT (input)	ρ*	M_1	M_2	M_3	P/kT eq 3.5	P/kT eq 3.4
			Function a				
256	0.31	0.20	0.997	0.996	0.996	0.31	0.31
500	0.31	0.20	0.997	0.996	0.996	0.32	0.32
256	0.90	0.39	0.993	0.987	0.984	0.92	0.92
500	0.90	0.39	0.993	0.988	0.984	0.92	0.92
256	2.40	0.59	0.985	0.972	0.961	2.33	2.33
500	2.40	0.61	0.985	0.971	0.960	2.45	2.46
256	6.16	0.85	0.970	0.942	0.916	6.13	6.14
500	6.16	0.85	0.970	0.943	0.917	6.04	6.06
			Function c				
256	0.37	0.20	1.108	1.233	1.380	0.37	0.37
500	0.37	0.20	1.107	1.232	1.378	0.38	0.39
256	1.36	0.40	1.085	1.182	1.292	1.36	1.37
500	1.36	0.41	1.084	1.180	1.288	1.43	1.43
256	3.66	0.60	1.062	1.130	1.205	3.68	3.69
500	3.66	0.61	1.062	1.130	1.204	3.76	3.77

[a] M_i, the ith moment of $F(\sigma)$, is shown as a function of density. The last two columns are the approximations eq 3.5 and 3.4, respectively.

function c at the highest packing fraction, corresponding to $\rho^* = 0.6$, the method fails suddenly for $\sigma_t > 1.3$.

Approximate chemical potential distributions can be obtained from scaled particle theory by using the first three moments of $F(\sigma)$,[3]

$$\mu^{ex}(\sigma) = -\ln(1-\xi_3) + (\sigma^3\xi_0 + 3\sigma^2\xi_1 + 3\sigma\xi_2)/(1-\xi_3) + (3\sigma^2\xi_1\xi_2 + (9/2)\sigma^2\xi_2^2)/(1-\xi_3)^2 + (3\sigma^2\xi_2^3)/(1-\xi_3)^3 \quad (3.2)$$

where

$$\xi_i = \pi\rho^* M_i/6 \quad (3.3)$$

The simulated moments can be used in eq 3.2 to estimate μ_{ex}^*. The excess chemical potential from the scaled particle theory is in excellent agreement with the simulation results for function a at all densities. For function c there are differences between theory and simulation at the highest value of ρ^*. This simulation corresponds to a higher packing fraction than the corresponding simulation of function a at the same number density. The disagreement may reflect inaccuracies in the simulated chemical potentials at this packing fraction or a failure of the scaled particle theory. It is clear from Figures 3 and 4 that eq 3.2 is a useful functional form for extrapolating simulated chemical potentials to higher packing fractions.

The pressure is more difficult to estimate in the canonical ensemble. The normal method would require the extrapolation of a large number of radial distribution functions, $g_{ij}(r_{ij})$, to contact at σ_{ij}, and a summation or integral over these weighted contact values. This route does not offer an accurate estimate of the pressure. We have also attempted to extend the method of Eppenga and Frenkel[26] but were unable to obtain accurate results with this technique. To solve this problem we performed a number of simulations in the isothermal isobaric ensemble.[24] This method is similar to that described in section 2 for variable polydispersity except that we allow volume fluctuations. The pressure is an input parameter and the number density is obtained as an ensemble average. Table III gives the results for functions a and c in the constant-NPT ensemble. System size checks are in excellent agreement and a comparison with the results in Table II indicates that the moments of $F(\sigma)$ are independent of the choice of ensemble.

The moments from the simulation can be used in two approximate equations to estimate the input pressure. The first approximation is the Carnahan–Starling equation for a monodisperse hard-sphere liquid at the same packing fraction, ξ_3, as the polydisperse fluid.

$$P/\rho kT = (1 + \xi_3 + \xi_3^2 - \xi_3^3)/(1-\xi_3)^3 \quad (3.4)$$

TABLE IV: Constant-NVT Simulation for Size Polydispersity in the Lennard-Jones Fluid[a]

ρ*	N	M_1	M_2	M_3	U*	P*
		Function a				
0.00		1.000	1.002	1.006		
0.005	256	1.000	1.002	1.005	−0.04	0.01
0.2	256	1.002	1.006	1.011	−1.50	0.14
0.4	256	1.002	1.006	1.012	−2.79	0.15
0.55	256	1.001	1.003	1.007	−3.72	0.30
0.55	500	1.001	1.004	1.009	−3.73	0.30
0.6	256	1.000	1.002	1.006	−4.04	0.48
0.6	108	1.001	1.003	1.007	−4.04	0.44
0.7	256	0.997	0.996	0.996	−4.64	1.09
0.8	256	0.992	0.985	0.980	−5.16	2.29
0.8[b]	256	0.991	0.984	0.979	−5.14	2.32
0.85	256	0.989	0.979	0.971	−5.35	3.23
0.85	500	0.989	0.980	0.973	−5.36	3.18
		Function c				
0.0		1.124	1.271	1.447		
0.005	256	1.124	1.272	1.448	−0.05	0.01
0.05	256	1.128	1.279	1.462	−0.55	0.05
0.1	256	1.131	1.288	1.478	−1.10	0.08
0.2	256	1.136	1.299	1.497	−2.08	0.10
0.2	500	1.137	1.301	1.501	−2.09	0.10
0.2[b]	256	1.136	1.300	1.498	−2.05	0.10
0.2[c]	256	1.136	1.299	1.496	−2.11	0.10
0.3	256	1.137	1.302	1.503	−2.98	0.11
0.4	256	1.130	1.286	1.474	−3.85	0.25
0.6	256	1.097	1.209	1.338	−5.12	1.72
0.8	500	1.068	1.143	1.225	−6.26	4.42
0.85	500	1.061	1.127	1.199	−6.43	5.65
0.85	864	1.061	1.128	1.200	−6.45	5.62
		Function b				
0.0		0.991	1.023	1.095		
0.005	500	0.991	1.022	1.093	−0.04	0.01
0.3	500	1.064	1.175	1.343	−2.54	0.09
0.8	500	0.946	0.924	0.933	−4.78	1.33

[a] Moments of $F(\sigma)$ as a function of density. All simulations are performed at $T^* = 1.35$. [b] A conventional Metropolis MC simulation. [c] A uniform starting distribution of sizes.

The second approximation is the extension of the Carnahan–Starling equation to polydisperse fluids by Salacuse and Stell[3]

$$P/kT = (6/\pi)[(\xi_0/(1-\xi_3)) + (3\xi_1\xi_2/(1-\xi_3)^2) + (3\xi_2^3/(1-\xi_3)^3) - (\xi_3\xi_2^3/(1-\xi_3)^3)] \quad (3.5)$$

Equation 3.4 requires a knowledge of the third moment, and eq 3.5 requires the first three moments. Within the accuracy with which we can calculate the number density and the moments, eq 3.4 and 3.5 give the same results which are in reasonable agreement with the input pressures over the whole density range for both distributions. It is clear from the system size checks presented in Table III that small differences in the final density and moments can produce significant differences in the pressures obtained from the approximations eq 3.4 and 3.5.

To understand the role of attractive forces in variable polydispersity we have performed simulations using the Lennard-Jones potential and three underlying distribution functions ((a), (b), and (c)). In Table IV, we present the moments, energy, and pressure from these simulations. The table contains a number of system size checks, and two simulations performed by using the conventional Metropolis MC method as well as the smart method. In addition all of the simulations were started from a monodisperse configuration. We include one simulation started from a uniform distribution of particle diameters, performed by using a smart sampling method. As expected, the results are independent of size, algorithm, and the initial configuration. For the three model distributions we observe an increase followed by a decrease in all the moments. The narrow symmetric distribution, function a, produces a 0.3% increase in packing fraction at $\rho^* = 0.55$, and a 3.5% decrease at $\rho^* = 0.85$. The distribution as a function of density is shown in Figure 5a. The shape remains essentially Gaussian. There is a small shift to the right at $\rho^* = 0.2$. At ρ^*

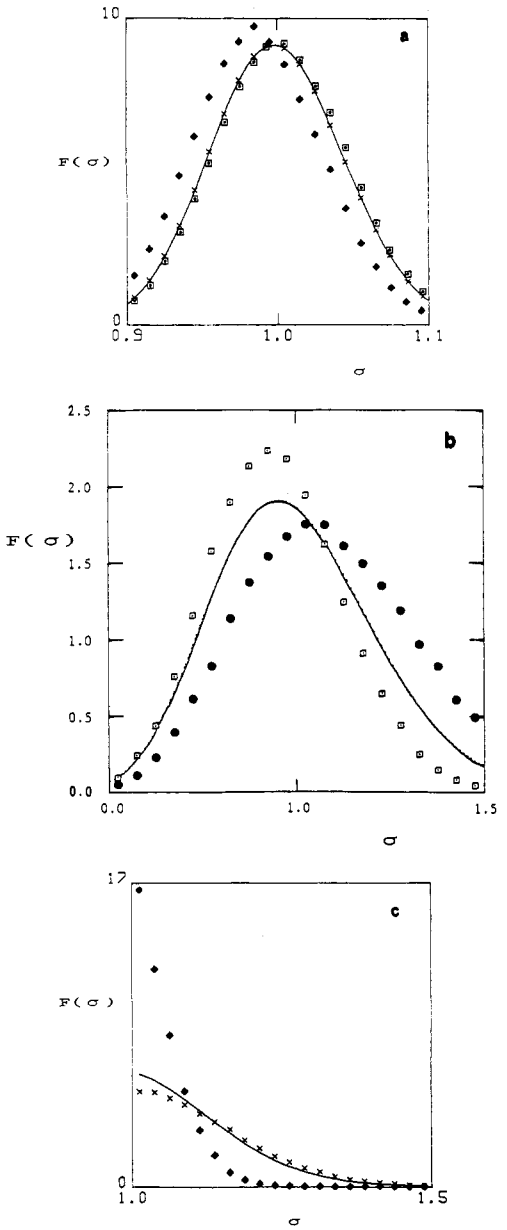

Figure 5. $F(\sigma)$ for the Lennard-Jones fluid as a function of density at $T^* = 1.35$: (a) function a, (—) $F_u(\sigma)$, (⊡) $\rho^* = 0.2$, (×) $\rho^* = 0.55$, and (◆) $\rho^* = 0.85$; (b) function b, (—) $F_u(\sigma)$, (●) $\rho^* = 0.3$, and (⊡) $\rho^* = 0.8$; (c) function c, (—) $F_u(\sigma)$, (×) $\rho^* = 0.2$, and (◆) $\rho^* = 0.85$.

TABLE V: Constant-NVT Simulations of Size Polydispersity in the Lennard-Jones Fluid[a]

T^*	M_1	M_2	M_3
	Function a		
1.0	0.993	0.987	0.983
1.35	0.989	0.979	0.971
2.0	0.986	0.973	0.963
3.0	0.985	0.971	0.959
4.0	0.985	0.971	0.959

[a] The moments of $F(\sigma)$ as a function of temperature at $\rho^* = 0.85$.

$= 0.55$ it returns to $F_u(\sigma)$, and by $\rho^* = 0.85$ it has moved to the left. With function b the same trends are observed, but now the packing fraction increase is 22.7% at $\rho^* = 0.3$, and the decrease is 14.8% at $\rho^* = 0.8$. In this case the upper cutoff b in $F(\sigma)$ limits the size increase with increasing density (see Figure 5b). The overall Gaussian shape is still retained. For the asymmetric distribution, function c, the increase in the packing fraction is 3.9% at $\rho^* = 0.3$, and the decrease is 17.1% at $\rho^* = 0.85$. In Figure 5c, we see a significant change in shape as the particle diameters decrease.

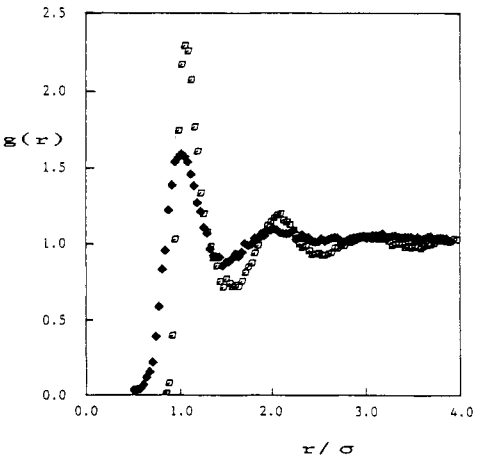

Figure 6. Average radial distribution function for the polydisperse Lennard-Jones fluids at $\rho^* = 0.8$, $T^* = 1.35$: (⊡) function a and (◆) function b.

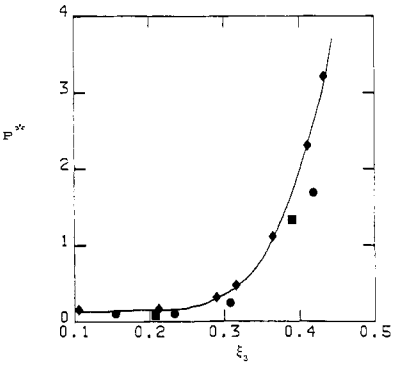

Figure 7. Lennard-Jones fluids pressure as a function of packing fraction at $T^* = 1.35$: (—) monodisperse, (◆) function a, (■) function b, and (●) function c.

In the Lennard-Jones fluid the distribution function, $F(\sigma)$, changes with temperature. Table V shows this effect for distribution function a. As the temperature increases the average particle size decreases. The moments appear to reach a limiting value at $T^* \approx 2.0$. If we use the mean diameter of the Lennard-Jones fluid at $\rho^* = 0.85$, $T^* = 2.0$ to obtain an average hard-sphere diameter using the WCA criterion, we obtain a mean hard-sphere diameter of 0.971, precisely the first moment of the polydisperse hard-sphere fluid at the same density (see Table II).

Figure 6 shows the average radial distribution function of two of the polydisperse Lennard-Jones fluids at $\rho^* = 0.8$, $T^* = 1.35$. The crosses denote function a, the dots function b. We recall that the average radial distribution function is a coarse measure of the structure obtained by sorting particles regardless of their diameter. For function a, the narrow symmetric distribution, we find that the average radial distribution function is very similar to $g(r)$ for a monodisperse fluid at the same packing fraction. For function b, the broader distribution, the packing fraction of the fluid (0.39) is somewhat less than for function a (0.41). This is a small difference in packing fraction, but the structure of the fluid for functions a and b is quite different. In other words, the structure of the fluid with a large degree of polydispersity cannot be represented by the structure of an effective monodisperse fluid at the same packing fraction. The large degree of polydispersity results in a loss of structure in $g(r)$ for $r > b$, the maximum particle size.

Figure 7 shows the pressure of the Lennard-Jones fluid as a function of packing fraction for distributions a, b, and c. The line represents the results for a monodisperse Lennard-Jones fluid. For a small degree of polydispersity, as in function a, the pressure is unaffected by the polydispersity; for the larger degrees of polydispersity, functions b and c, the pressure lies below the monodisperse result.

Two forms for $F_u(\epsilon)$ were used in our study of energy polydispersity, function a (Table I) with σ replaced by ϵ and function

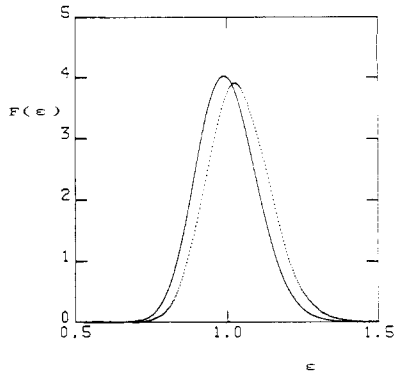

Figure 8. $F(\epsilon)$ against ϵ for the Lennard-Jones fluid at $T^* = 1.35$. The line is the underlying distribution function d, and (···) at $\rho^* = 0.8$.

TABLE VI: Constant-NVT Simulation Results for Energy Polydispersity in the Lennard-Jones Fluid at $T^* = 1.35$[a]

ρ^*	N	$(M_{1/2})^2$	M_1	M_2	M_3	U^*	P^*
			Function a				
0.0			1.000	1.002	1.006		
0.2	256	1.002	1.002	1.005	1.011	−1.50	0.14
0.5	256	1.004	1.004	1.010	1.017	−3.39	0.20
0.8	256	1.006	1.007	1.015	1.025	−5.28	2.62
			Function d				
0.0			1.000	1.010	1.030		
0.2	256	1.008	1.011	1.032	1.064	−1.52	0.14
0.4	256	1.018	1.020	1.051	1.094	−2.81	0.14
0.6	256	1.027	1.029	1.070	1.123	−4.16	0.41
0.8	256	1.036	1.039	1.090	1.155	−5.49	2.42
0.8	1.08	1.036	1.038	1.089	1.153	−5.48	2.42

[a] The moments and thermodynamic properties are presented as a function of density.

d, $z = 100$, $a = 0.5$, and $b = 1.5$, with $\tau = 0.100$. The results are given in Table VI where we see that the average well depth increases continuously with increasing density and in Figure 8 we show the form of $F(\epsilon)$ at $\rho^* = 0.8$, using function d.

The results in Table VI for function a show only a slight deviation from the properties of the monodisperse Lennard-Jones liquid at the same number density. This can be explained by using a simple perturbation approach. The reference system consists of Lennard-Jones particles, all with a well depth equal to the first moment, M_1, of the distribution $F(\epsilon)$. The perturbation can be written as the change in the free energy of the liquid associated with the particles having specific well depths, which are different from the mean value

$$A/NkT = (A_{ref}[T,N,M_1]/NkT) + 2\pi\rho\beta\int_0^\infty d\epsilon_i\, F(\epsilon_i) \times \int_0^\infty d\epsilon_j\, F(\epsilon_j) \int_0^\infty (V(\epsilon_i,\epsilon_j,r) - V(M_1,r))\, g(T,M_1,\rho) r^2\, dr \quad (3.6)$$

$$(A - A_{ref})/NkT = 8\pi\rho\beta\int_0^\infty d\epsilon_i\, F(\epsilon_i) \int_0^\infty d\epsilon_j\, F(\epsilon_j)(\epsilon_i\epsilon_j)^{1/2} - M_1) \int_0^\infty [(\sigma/r)^{12} - (\sigma/r)^6] g(T,M_1,\rho) r^2\, dr \quad (3.7)$$

The thermodynamic properties of the polydisperse liquid will be the same as those of the monodisperse liquid if the square of the half-moment is equal to the first moment of $F(\epsilon)$ at a particular density and temperature. The results in Table VI show that this is the case for function a but that this does not apply to the wider function b.

4. Theory

In this section we shall develop a theory for the final distribution $F(\sigma)$ in terms of the underlying distribution function in the case of variable size polydispersity. There is a single-particle energy, $V_{intra}(\sigma)$, associated with a particular diameter. In the framework of a density functional theory,[28] there is a total free energy consisting of two terms; an interparticle contribution including an ideal gas and an excess part, and an intraparticle contribution depending on $V_{intra}(\sigma)$.

$$A = A_{inter} + A_{intra}$$

$$A = A_{inter}(\rho,F(\sigma)) + N\int_0^\infty V_{intra}(\sigma)\, F(\sigma)\, d\sigma \quad (4.1)$$

The free energy must be minimized with respect to $F(\sigma)$ with the constraint of a fixed number of particles.

$$\delta A/\delta F(\sigma) - N\mu = \delta A_{inter}/\delta F(\sigma) + NV_{intra}(\sigma) - N\mu = 0 = N(\mu_{inter}(\sigma) + V_{intra}(\sigma) - \mu) = 0 \quad (4.2)$$

The Lagrange multiplier, μ, is the chemical potential of the particles and $\mu_{inter}(\sigma)$ is the chemical potential of a particle of diameter σ when the particle distribution is fixed at $F(\sigma)$. Equation 4.2 is the central equation in the theory and is analogous to the fundamental equation for micelle equilibrium.[14] The crucial input is the interparticle free energy for a polydisperse fluid, $A_{inter}(F(\sigma))$, which has been studied by a number of authors.[6,8]

4.1. The Low-Density Limit. In the low-density limit, A_{inter} is given by the ideal gas contribution

$$A_{inter}/NkT = A_{id}/NkT = \int_0^\infty F(\sigma)\, \ln(\Lambda^3\rho F(\sigma))\, d\sigma \quad (4.3)$$

where Λ is the de Broglie wavelength and hence

$$\mu_{inter}(\sigma)/kT = 1 + \ln \Lambda^3\rho F(\sigma) \quad (4.4)$$

Using eq 4.2 we obtain

$$kT \ln \rho F(\sigma) + V_{intra}(\sigma) = \text{constant} \quad (4.5)$$

As expected

$$F(\sigma) \propto \exp(-V_{intra}(\sigma)/kT) \quad (4.6)$$

The definition of $V_{intra}(\sigma)$ is equivalent to definition of the low-density limit of $F(\sigma)$, the underlying distribution function $F_u(\sigma)$. In many cases $V_{intra}(\sigma)$ is harmonic about the underlying mean diameter σ_0, and

$$F_u(\sigma) \propto \exp(-(L/2kT)(\sigma - \sigma_0)^2) \quad (4.7)$$

where L is a kind of elastic constant. Equation 4.7 can be written in a normalized form

$$F_u(\sigma) = (1/2\pi s_0^2)^{1/2} \exp(-(\sigma - \sigma_0)^2/2s_0^2) \quad (4.8)$$

where the standard deviation, s_0, is given by $(kT/L)^{1/2}$. This is an harmonic approximation to the Schultz functions discussed in sections 1–3. Helfrich[29] uses a similar concept in discussing the susceptibility of a micelle to expansion or contraction: he defines the surface rigidity K by

$$K = (kT/4\pi)(\sigma/s_0)^2 \quad (4.9)$$

4.2. Fluid Densities. At fluid densities we use a perturbation approach to determine the interparticle contribution to the free energy. For the reference system we use a polydisperse hard-sphere fluid, described by the Mansoori–Carnahan–Starling–Leland approximation.[30]

$$A_{ex}^{HS}/NkT = [(\xi_2^3/\xi_0\xi_3^2) - 1] \ln(1 - \xi_3) + 3\xi_1\xi_2/\xi_0(1 - \xi_3) + \xi_2^3/\xi_3\xi_0(1 - \xi_3)^2 \quad (4.10)$$

where the ξ_i are given in eq 3.3. If we consider an additional attractive long-range potential then

$$A_{inter}(\rho,F(\sigma),T) = A_{id} + A_{ex}^{HS} + A_{ex}^{LR} \quad (4.11)$$

(28) Sluckin, T. *Mol Phys.* **1981**, *43*, 817. Evans, R. *Adv. Phys.* **1979**, *28*, 143.
(29) Helfrich, W. *J. Phys.* **1973**, *C28*, 693.
(30) Mansoori, G. A.; Carnahan, N. F.; Starling, K. E.; Leyland, Jr. T. W. *J. Chem. Phys.* **1971**, *54*, 1523.

In the random-phase approximation[31]

$$A_{ex}^{LR}/NkT = 2\pi\beta\int_0^\infty\int d\sigma_i\, d\sigma_j\, F(\sigma_i)\, F(\sigma_j)\int_{(\sigma_i+\sigma_j)/2}^\infty V^{LR}(r_{ij})\, dr_{ij} \quad (4.12)$$

where V^{LR} is the attractive part of the Lennard-Jones potential using the Weeks, Chandler, and Andersen split. Equation 4.12 can be evaluated to give

$$A_{LR}/NkT = 0.462\pi\beta\rho\epsilon(M_3 + 3M_2M_1)$$
$$= 2.771\epsilon\beta(\xi_3 + (3\xi_2\xi_1/\xi_0)) \quad (4.13)$$

Equations 4.3, 4.10, and 4.13 are a simple model for the free energy as a functional of $F(\sigma)$. In principle, $F(\sigma)$ can now be found at any temperature and density by solving the functional Euler–Lagrange equations (4.2) for a fixed $V_{intra}(\sigma)$ or $F_u(\sigma)$. In practice, a further simplification facilitates the calculation and promotes our understanding of the model.

4.3. Analytical Approximation to the Euler–Lagrange Equation. We propose two different forms for $V_{intra}(\sigma)$. Form A is given by

$$V_{intra}(\sigma)/kT = V_{intra}(\sigma_0)/kT + (\sigma - \sigma_0)^2/2s_0^2$$

where $V_{intra}(\sigma_0)$ is an energy scaling factor which can be set to zero. In this case the underlying distribution function is

$$F_u(\sigma) = (1/(2\pi s_0^2)^{1/2})\exp(-(\sigma - \sigma_0)^2/2s_0^2) \quad (4.14)$$

Form B has a minimum diameter

$$V_{intra}(\sigma)/kT = \infty \qquad \sigma < \sigma_0$$
$$= (\sigma - \sigma_0)^2/2s_0^2 \qquad \sigma > \sigma_0$$

and the underlying distribution function is

$$F_u(\sigma) = 0 \qquad \sigma < \sigma_0$$
$$= (2/(2\pi s_0^2)^{1/2})\exp(-(\sigma - \sigma_0)^2/2s_0^2) \qquad \sigma > \sigma_0 \quad (4.15)$$

We can approximate the underlying Schultz distributions a and c used in section 3 with the Gaussian form A and half-Gaussian form B. Within the harmonic approximation σ_0 is equivalent to the mean diameter of the underlying Schultz distribution, and s_0 can be identified with the standard deviation of $F_u(\sigma)$. These Gaussian forms facilitate the analysis. To further simplify the calculation we postulate a functional form for the final distribution $F(\sigma)$ which depends on a few parameters. We can then determine the free energy at a given density as a function of these parameters and solve the Euler–Lagrange equations to determine how the distribution function $F(\sigma)$ changes with density and temperature.

In the case of form A, we postulate that

$$F(\sigma) = (2\pi s^2)^{-1/2}\exp[-(\sigma - \sigma_0 - \sigma_1)^2/2s^2] \quad (4.16)$$

The mean diameter is shifted from σ_0 to $\sigma_0 + \sigma_1$, and the standard deviation changes from s_0 to $s = (M_2 - M_1^2)^{1/2}$. It is convenient to use reduced units in which $\sigma_0 = 1$ and to suppose that the distribution is narrow so that we can make an expansion in powers of s. We obtain

$$A_{intra}/NkT = (\sigma_1^2 + s^2)/2s_0^2$$

$$A_{id}/NkT = \ln\Lambda^3\rho - \tfrac{1}{2}\ln(2\pi e) - \ln(s)$$

$$A_{ex}^{HS}/NkT = P(4 - 3P)/(1 - P)^2 + (s^2/M_1^2)[-3\ln(1 - P) + 9P^2/(1 - P)^2 + 6P^2/(1 - P)^3 + 3P/(1 - P)] + \ldots$$

$$A_{ex}^{LR}/NkT = -11.086\epsilon\beta P - (s^2/M_1^2)[16.628\epsilon\beta P] + \ldots \quad (4.17)$$

where P is the packing fraction of the polydisperse fluid and an equivalent monodisperse fluid at the same number density with a mean diameter $M_1 = \sigma_0 + \sigma_1 = 1 + \sigma_1$, $P = (\pi/6)\rho^*M_1^3$. A_{ex} has been written as an expansion in powers of s/M_1. The polydispersity is accounted for by the term in A_{ex} of $O(s/M_1)^2$. The appropriate Euler–Lagrange equations are

$$\partial A/\partial\sigma_1 = 0$$
$$\partial A/\partial s = 0 \quad (4.18)$$

Within the spirit of a first-order perturbation theory these equations give

$$\sigma_1 = s_0^2[-12\xi_0(1 - 0.5\xi_0)/(1 - \xi_0)^3 + 33.258\epsilon\beta\xi_0] \quad (4.19)$$

$$1/s^2 = 1/s_0^2 + 2[-3\ln(1 - \xi_0) + 9\xi_0^2/(1 - \xi_0)^2 + 6\xi_0^2/(1 - \xi_0)^3 + 3\xi_0/(1 - \xi_0) - 16.628\epsilon\beta\xi_0] \quad (4.20)$$

where $\xi_0 = \pi\rho^*/6$ is the packing fraction of a monodisperse fluid of unit size at the density ρ^*.

The shift in the particle diameter is of $O(s_0^2)$ and consists of a negative part from the hard-sphere repulsive potential and a positive part from the attractive interaction. At high temperatures the size decrease resulting from the hard-core repulsion dominates at all densities. In contrast eq 4.19 shows that in the theory for $T^* = kT/\epsilon < 2.77$, the particle size initially increases at low densities before decreasing at higher densities. This temperature is considerably above the critical temperature for the monodisperse Lennard-jones fluid in the RPA which is $T_c^* = 1.09$. The results from eq 4.19 are compared with simulation in Table VII. In the case of the symmetric distribution, the standard deviation s_0 is given by $(M_2 - M_1^2)^{1/2}$ using the moments of $F_u(\sigma)$ in Table I. The agreement between theory and simulation for the hard-sphere and the Lennard-Jones models is good up to $\rho^* = 0.6$. At higher densities the theoretical diameter falls too quickly in both cases. This agreement indicates that this simple theory contains the essential physics of the problem. Equation 4.20 determines the change in s as a function of density. The theory predicts a very

TABLE VII: M_1 and s as a Function of Density from Theory and Simulation for the Polydisperse Hard-Sphere and Lennard-Jones Fluids with $F_u(\sigma)$ for Function a and M_1 for Function c from Simulation and Theory

	M_1		s	
ρ^*	theory	simuln	theory	simuln
	Hard-Sphere Fluids, Function a			
0.0	1.000	1.000	0.045	0.045
0.2	0.997	0.998	0.045	0.032
0.4	0.991	0.993	0.045	0.031
0.6	0.980	0.985	0.044	0.042
0.85	0.944	0.970	0.043	0.033
	Lennard-Jones Fluids, Function a			
0.0	1.000	1.000	0.045	0.045
0.2	1.002	1.002	0.045	0.045
0.4	1.001	1.002	0.045	0.045
0.55	0.997	1.001	0.045	0.032
0.6	0.995	1.000	0.045	0.045
0.7	0.988	0.997	0.044	0.045
0.8	0.974	0.991	0.044	0.031
0.85	0.970	0.989	0.044	0.030

	M_1		
ρ^*	theory[a]	theory[b]	simuln
	Hard-Sphere Fluids, Function c		
0.0	1.124	1.124	1.124
0.2	1.120	1.107	1.107
0.4	1.111	1.068	1.085
0.6	1.091	0.962	1.062
	Lennard-Jones Fluids, Function c		
0.0	1.124	1.124	1.124
0.05	1.125	1.127	1.128
0.1	1.125	1.129	1.131
0.2	1.126	1.130	1.136
0.3	1.125	1.126	1.137
0.4	1.123	1.113	1.130
0.6	1.110	1.030	1.097
0.8	1.067	0.693	1.068
0.85	1.046	0.487	1.061

[a] s_0 from M_1 and M_2 of $F_u(\sigma)$. [b] s_0 from eq 4.24.

(31) Evans, R.; Sluckin, T. J. *J. Phys.* **1981**, *C14*, 2569.

small decrease in s with density for both models. However, as s_0 is itself small, and the change is a factor of s_0^2 smaller than this, s is effectively constant for function a. The simulated moments can be obtained with an accuracy of 0.3% and this is not accurate enough to determine a trend in the simulated s.

In modelling form B, the asymmetric distribution, we take a different approach. We parametrize the distribution using s, the standard deviation.

$$F(\sigma) = (2/(2\pi s^2)^{1/2}) \exp(-(\sigma - \sigma_0)^2/2s^2) \qquad \sigma > \sigma_0$$
$$= 0 \qquad \sigma < \sigma_0 \tag{4.21}$$

This parametrization is quite different from that of eq 4.16. Unlike the symmetric distribution we do not build a shift in the mean into the functional form by including a term in σ_1. We recognize that $F(\sigma)$ remains a decreasing function of σ for $\sigma > \sigma_0$ and that it is a variation in s which affects the average particle diameter. We are no longer able to make the approximation implicit in eq 4.19 that the polydisperse fluid can be represented as a monodisperse fluid of particles with a variable effective diameter.

In this case we use eq 4.10 and 4.13, with the ideal gas contribution to the Helmholtz free energy, to express A in terms of $\xi_i(s)$. Minimizing A with respect to s and setting $\sigma_0 = 1$ gives

$$s^2 = s_0^2(1 - Gs) \tag{4.22}$$

where

$$G = 2.394(1 + 2.51s + 2.0s^2)[-\xi_2^3/\xi_3^2(1 - \xi_3) - 2 \ln (1 - \xi_3)\xi_2^3/\xi_3^3 + \xi_0/(1 - \xi_3) + 3\xi_1\xi_2/(1 - \xi_3)^2 + 2\xi_2^3/\xi_3(1 - \xi_3)^3 - \xi_2^3/\xi_3^2(1 - \xi_3)^2] + 1.60(1 + 1.25s) \times [3 \ln (1 - \xi_3)\xi_2^2/\xi_3^2 + 3\xi_1/(1 - \xi_3) + 3\xi_2^2/\xi_3(1 - \xi_3)^2] + 0.798[3\xi_2/(1 - \xi_3)] - 26.55[1 + 2.05s + 1.25s^2]\epsilon\beta\xi_0 \tag{4.23}$$

This gives an average diameter of

$$M_1 = 1 + 0.798s \tag{4.24}$$

and a shift in diameter of

$$\sigma_1 = -0.339Gs_0^2 + O(s_0^3) \tag{4.25}$$

As in the case of form B the hard-sphere contributions decrease the average diameter and the attractive interactions increase the particle size. The mean diameters obtained from eq 4.25 are compared with the simulation results in Table VII. One difficulty with the theory in this case is the choice of s_0. We can use the value determined directly from the moments of $F_u(\sigma)$ or fit eq 4.24 to the first moment of $F_u(\sigma)$. It is clear from Table VII that the second choice is more consistent at lower densities. The agreement is reasonable up to $\rho^* = 0.4$, but again the theoretical diameters fall too quickly at higher densities. The theory makes no prediction for the change of standard deviation as a function of density.

In the case of the hard-sphere fluids we have used an empirically well-established formula for the free energy in terms of the moments of the expected diameters. Unsurprisingly, there is a free-energy cost in increasing the density which can be reduced by making the particles smaller. This is balanced by the changes in intraparticle energy, and the net result is a decrease in the average particle size. The theory agrees quantitatively with the simulations at low density and is poorer at higher packing fractions. We believe that the agreement could be improved by including interparticle correlations and by a more accurate match of the underlying distributions in the theory and the simulation. For the Lennard-Jones particles the theory predicts an initial increase in size followed by a decrease, and the results are in qualitative agreement with those obtained from the simulation.

5. Conclusions

The present work demonstrates that it is possible to simulate a polydisperse fluid by assuming a form for the self (intraparticle)-energy at low densities and using a modified Metropolis Monte Carlo algorithm to account for interparticle effects.

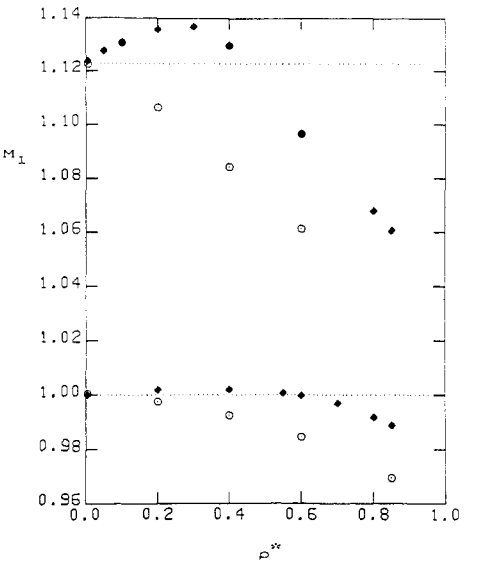

Figure 9. Average particle diameter against reduced density for the polydisperse Lennard-Jones and hard-sphere fluids, functions a and c.

For fluids of hard-sphere particles the average size of the particles decreases with increasing density for a fixed number of particles. For fluids of Lennard-Jones atoms the interparticle attractions initially cause the mean particle size to increase with increasing density before it decreases at higher density. This phenomenon is shown in Figure 9 where we have plotted the first moment of the fluid as a function of density for hard-sphere and Lennard-Jones fluids using the underlying distribution functions a and c. The initial increase in particle size becomes less significant at higher temperatures.

The simulations also show that for small degrees of polydispersity the thermodynamics of the fluid can be well understood in terms of an effective monodisperse fluid. We have developed a density functional theory of these phenomena, which can be solved analytically within the framework of first-order perturbation theory. The theory is in reasonable qualitative agreement with the simulations.

The methods proposed in this paper are expected to be useful in a wide range of phenomena exhibiting variable polydispersity. In addition to colloidal dispersions, micellar solutions, and microemulsions, we note that this phenomenon occurs in metals or salts where the effective unit changes as a function of density, and also in ordinary matter at neutron-type densities. As long as the intraparticle configuration space is completely spanned by the low-density distribution the response of particles to the interparticle forces can be predicted.

Note Added in Proof. Glandt[32] has recently pointed out that eq 3.1, the Widom particle insertion equation in the constant-NVT ensemble, should be slightly modified for application in the semi-grand-ensemble. The results from these two formulas agree to within our estimated error of 4% in the chemical potential calculation.

Acknowledgment. M.S. thanks SERC and British Petroleum for a CASE award. D.J.T. and N.Q. thank British Petroleum International, Sunbury on Thames, for supporting their collaborative research. T.S. thanks Philippe Nozieres for his hospitality at the I.L.L. and the Lady Davis Foundation for financial support at the Technion where part of this work was carried out. N.Q. thanks BP plc for permission to publish.

(32) Kofke, D. A.; Glandt, E. D. *J. Chem. Phys.* **1987**, *87*, 4881.